

Fluidization and anomalous density fluctuations in epithelial tissues with pulsating activity

Zhu-Qin Li,¹ Qun-Li Lei,^{1, 2, 3, *} and Yu-qiang Ma^{1, 2, 3, †}

¹*National Laboratory of Solid State Microstructures and School of Physics,
Collaborative Innovation Center of Advanced Microstructures,
Nanjing University, Nanjing 210093, People's Republic of China*

²*Jiangsu Physical Science Research Center, Nanjing 210093, People's Republic of China*

³*Hefei National Laboratory, Hefei 230088, People's Republic of China*

Cells not only have self-motility by crawling but are also capable of other types of active motions like periodic contraction or pulsation. In this work, by using the Voronoi cell model, we show how this non-motility activity affects the structure, dynamic and density fluctuations of cellular monolayers. We find that random cell pulsation can fluidize solid epithelial tissues, resulting in *hyperuniform* fluids, while pulsation synchronization inhibits the fluidity and causes a reversed solidification. We prove this solidification is a BKT-type transition, characterized by strong density/dynamic heterogeneity arising from the birth of topological defects in the pulsating phase space. The magnitude and length scale of density heterogeneity diverge with the pulsating period, resulting in an opposite *giant* density fluctuation. We propose an unified fluctuating hydrodynamic theory to explain the two very different anomalous density fluctuations phenomena. Our findings can help understanding recent experimental observations in MDCK monolayers.

INTRODUCTION

Collective motions of cells in epithelial tissues underlies many vital life processes, like embryonic development, wound healing and cancer invasion [1–3], which are associated with the fluidization of epithelial tissues [4–7] or flocking of cells [8, 9], etc. [10–13]. Previous studies focused on the role of self-motility of cells on these processes [6, 8–10, 14–16]. However, non-motility activities, e.g., active cell deformation or periodic pulsation [17–22], are also generic features of cell tissues. For example, pulsating contractions can be induced by actin and myosin dynamics [23–36], which are closely related to contraction waves, morphogenesis and pattern formations in epithelial tissues [37–42]. Meanwhile, pulsating activity can be caused by the exchange of fluid between cells [43, 44], or active nuclear movements [45]. During these active pulsating processes, synchronization has been observed [28, 43]. How pulsating activities and their synchronization affect the fluidity of epithelial tissues remains poorly understood. Moreover, epithelial tissues show *giant* density fluctuations driven by collective cell migration or cell pulsation [43, 46], while in other cellular systems, suppressed density fluctuations or *hyperuniform* states were reported [47–51]. Thus, it is also intriguing to reveal the connection between non-motility activities and anomalous density fluctuations in epithelial tissues.

In this work, we focus on the effects of pulsating activity on the structure, dynamic and density fluctuations of epithelial monolayers. Based on the Voronoi cell model, we find that random cell pulsation fluidizes epithelial tissues, generating a hyperuniform fluid state of class I hyperuniformity [52, 53]. When cell pulsations are synchronized, the fluid state is reversely solidified. This synchronization-induced solidification is a Berezinskii-

Kosterlitz-Thouless (BKT) type transition, where density and dynamic heterogeneity emerge at the transition point due to the birth of topological defects in the pulsating phase space. Both the magnitude and length scale of the density heterogeneity diverge with the pulsating period, which results in an opposite giant density fluctuations [54]. We generalize the underlying mechanism into an unified fluctuating hydrodynamic theory which explain the two very different anomalous density fluctuations phenomena. We also prove that above phenomena are insensitive to the form of pulsation, i.e., volume or tension pulsation. Our work provides a minimal model to understand recently observed giant density fluctuations and associated topological defects in MDCK monolayer [27, 28, 43].

RESULTS

Model We consider a 2D confluent cell monolayer composed of N pulsating cells whose area and shape can change with time (Fig. 1a). Cells are modelled as polygons determined by the Voronoi tessellation of the space [6]. We assume the pulsation is strong enough that the effect of thermal noise can be neglected in the overdamped cell dynamics. In our model, each cell i has the normalized preferred area a_0^i which does stochastic oscillation, i.e.,

$$a_0^i = 1 + \alpha \sin \varphi_i(t), \quad (1)$$

where α is the pulsating strength and $\varphi_i(t)$ is the pulsating phase. The normalized preferred perimeter is $p_0^i = p_0$ with p_0 the so-called *target shape factor* [6] characterizing the time averaged preferred shape of cell. The preferred area and perimeter of cells can not be all satisfied

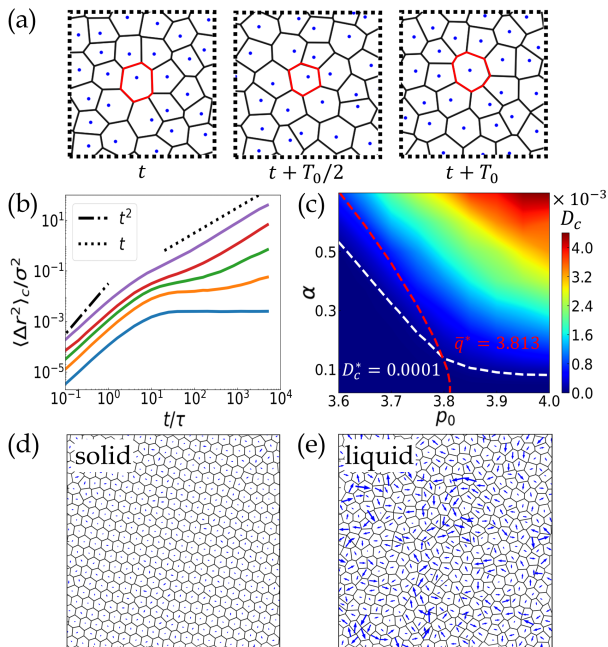


FIG. 1: (a) Schematics of a cell configuration (denoted in red) over a cell pulsating cycle T_0 . (b) MSD_c under fixed $p_0 = 3.7$ and different pulsating strength $\alpha = [0.1, 0.2, 0.3, 0.4, 0.7]$ (bottom to top). (c) Phase diagram of diffusion coefficient D_c . (d-e) Typical solid ($p_0 = 3.7, \alpha = 0.2$) and fluid ($p_0 = 3.7, \alpha = 0.6$) configurations. Blue arrows show the cell displacements after one period. All data are for random pulsation systems ($J = 0$).

in a confluent cell tissue, which gives rise to an effective energy determining the dynamics equation of cells (see Materials and Methods for details). Moreover, to account for collective cell pulsation, we assume $\varphi_i(t)$ obeys the stochastic Kuramoto-like dynamics [55–57], i.e.,

$$\frac{d\varphi_i}{dt} = \omega_0 + J \sum_{j \in C_i} \sin(\varphi_j - \varphi_i) + \sqrt{2T_\varphi} \eta_i(t), \quad (2)$$

where frequency ω_0 and the corresponding period $T_0 = 2\pi/\omega_0$ are supposed to be associated with certain intrinsic cell cycles or the intrinsic oscillation frequency induced by mechanochemical feedback [28, 43]. The second term represents the coupling between adjacent cells with J the coupling strength. T_φ is the noise strength in the phase space and $\eta_i(t)$ is Gaussian white noise. This simplified model is inspired from more sophisticated biological models while retaining the essential physics [18, 28]. Detail simulation information can be found in the Materials and Methods.

Cell-pulsation induced fluidization We first study the case of zero pulsation coupling ($J = 0$). To characterize the dynamical states of cellular monolayers, we calculate the cage relative mean square displacement of cells, $\text{MSD}_c(t)$, which excludes the influence of the long-wavelength fluctuations in 2D (Materials and Methods).

As shown in Fig. 1b, the plateau of MSD_c gradually disappears and exhibits diffusion scaling with increasing α . This indicates a pulsation-induced fluidization analogous to the one induced by motility [6]. Similar behaviors have been reported in the actively-deforming spherical particle system [17]. Microscopically, the fluidization arises from unbalanced intercellular forces induced by random pulsation, which results in frequent T1 transitions (Movie. S1). In Fig. 1c, we plot the diffusion coefficient D_c of systems in dimensions of α and p_0 , where the solid and liquid phases can be roughly separated by a threshold $D_c^* = 10^{-4} \sigma^2 / \tau$ [6]. It would be interesting to further study in detail the nature of this transition and the glass dynamics [58, 59]. We also confirm that the solid phase in our model has the crystal order (*SI Appendix*, Fig. S1b and Movie. S2). From Fig. 1c, one can see that systems with large p_0 are more easily fluidized as long as $\alpha \gtrsim 0.1$. This accords with the energy barrier scenario of T1 transition [5]. Nevertheless, by accurately calculating the average shape factor $\bar{q} = \sum_i (p_i / \sqrt{a_i}) / N$, we find the line of zero-energy-barrier, i.e., $\bar{q}^* = 3.813$ [5, 6], does not follow the trend of line D_c^* , especially for small α . This results in a phase regime with $p_0 > 3.8$ and $\alpha < 0.1$, in which cells are highly deformed (large \bar{q}) but their movements are arrested (little D_c). Similar states have also been observed experimentally in MDCK monolayer with low fluctuating edge tension [34].

Synchronization-induced solidification We further consider the intercellular coupling during pulsation. We find that increasing coupling strength J leads to a synchronization transition at $J^* \simeq 0.06\tau^{-1}$, above which cells pulsation are synchronized. The synchronization degree can be characterized by the phase polarity $M = \langle |\sum_i (\cos \varphi_i, \sin \varphi_i)| \rangle / N$ (Fig. 2a), which ranges from [0, 1]. We find that this synchronization transition is insensitive to the choice of α and p_0 (*SI Appendix*, Fig. S2a,c). To explore how the synchronization transition in the pulsating phase space affect the cell dynamics in real space, we further plot D_c in dimensions of J and p_0 at fixed $\alpha = 0.4$ in Fig. 2b. We find that for the liquid phase, D_c drops quickly as J increases above J^* , suggesting a synchronization-induced solidification. Compared with the unsynchronized states, the cell sizes in the synchronized states are more uniformly distributed (*SI Appendix*, Fig. S2d). Thus cells experience more balanced intercellular force during the collective pulsation. This suppresses the T1 transition and leads to the solidification.

Interestingly, near the synchronization transition point, we find the coexistence of high-density contracted regions and low-density expanded regions that periodically switch their states (Fig. 2c and Movie. S3). This density heterogeneity is strongest at J^* , as proven by the height of the first peak in structure factor $S(q)$ (Fig. 3c). In Fig. 2e, we also show that cell motility is negligible

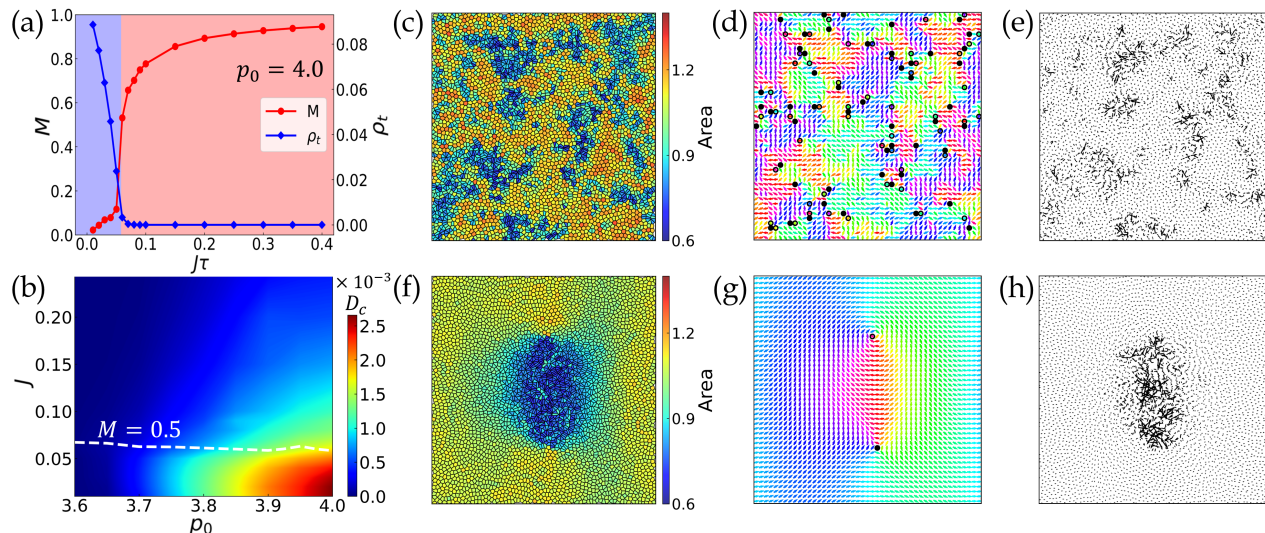


FIG. 2: (a) Phase polarization M (red line) and topological defect density ρ_t (blue line) as a function of J at fixed $p_0=4.0$, with transition point $J^* \simeq 0.06\tau^{-1}$. (b) Phase diagram of D_c at $\alpha=0.4$. The white dashed line represents states with $M=0.5$. (c) Cell area distribution for the system at $J=0.05\tau^{-1}$ and $p_0=4.0$. (d) The pulsating phase field for the same configuration in (c) with the color arrow indicates the phase. The solid circle and open circle represent the $+1$ and -1 topological defects, respectively. (e) Instantaneous velocity field for the configuration in (c). (f-h) The same figures as that in (c-e) for a pair of topological defects at $J=0.01\tau^{-1}$, $p_0=4.0$ and $T_\varphi=0$. For all simulations, $N=4096$.

like a solid in the expanded regions, while much higher akin to a liquid in the contracted regions. We find that this dynamic heterogeneity is a result of heterogeneous distribution of local shape factor $\bar{q}_i(t) = (p_i(t)/\sqrt{a_i(t)})$ which is large (small) in the contracted (expanded) regions. A larger (smaller) shape factor corresponds to a more anisotropic (isotropic) cell shape and stronger (weaker) imbalanced intercellular forces which favour the liquid (solid) phase [5, 6]. We notice that similar density heterogeneities and local synchronized pulsation patterns were observed in MDCK monolayers [25, 27, 43].

It is known that the (de-)synchronization transition described by Kuramoto model belongs to BKT universality, accompanied by the creation and annihilation of (± 1) topological defects. We confirm this scene by calculating the topological defect density $\rho_t = Q/N$ in the pulsating phase space (Fig. 2a). See *SI Appendix* for the identification method of topological defects. Furthermore, we plot the pulsating phase field of the cell monolayer near the critical point in Fig. 2d. We identify ± 1 topological defects and find they are mostly located on the boundaries between contracted and expanded regions. Similar pulsation phase topological defects have recently been identified in MDCK monolayer in experiments [28]. To further disclose the relationship between the topological defects and density/dynamic heterogeneities, we create a single pair of ± 1 topological defects in the pulsating phase space (See *SI Appendix*) and observe its evolution (Fig. 2f-h). We find that the topological defects create a synchronized cell droplet in between, which contracts (fluidizes) or expands (solidifies) alternatively. It also creates a local pulsating wave around the defect pair (Movie. S4).

Thus, the synchronization-induced solidification of the monolayers is essentially a BKT-type transition, resulting from the annihilation of topological defects in the pulsating phase space.

Anomalous density fluctuations Next, we focus on the density fluctuations of the pulsation system. As shown in Fig. 4, the static structure factor $S(q)$ for random pulsating tissue ($J=0$) in liquid state ($\alpha=0.4$) shows a scaling $S(q \rightarrow 0) \sim q^2$, a hallmark of class I hyperuniform state with vanishing density fluctuations at infinite wavelength [52, 53]. In order to study the effect of pulsating period T_0 on hyperuniformity, we plot the structure factor $S(q)$ for random pulsation systems under different T_0 and fixed $(p_0, \alpha) = (4.0, 0.4)$ in Fig. 3a. With decreasing T_0 , we find that the q^2 scaling remains unchanged, while the degree of hyperuniformity is enhanced. Decreasing α has a similar effect (Fig. 3b), but the relaxation dynamic would also be slower. Thus hyperuniformity is the strongest when cells undergo fast and weak pulsation in the liquid state.

In addition to the pulsating period T_0 and strength α , the synchronization of pulsation also affects the density fluctuations of the system. With increasing J from zero to J^* for system under $(p_0, \alpha) = (4.0, 0.4)$, we find that a new peak in $S(q)$ gradually develops around $q^* \sim 0.3 \sigma^{-1}$ without modifying q^2 scaling when $q \rightarrow 0$ (Fig. 3c). This indicates the coexistence of local large density fluctuations with global hyperuniformity, a scenario similar to circle swimmer systems [52]. Interestingly, with further increasing J , the height of the peak denoted as S_{max} gradually decreases. This is best shown in Fig. 3e, where

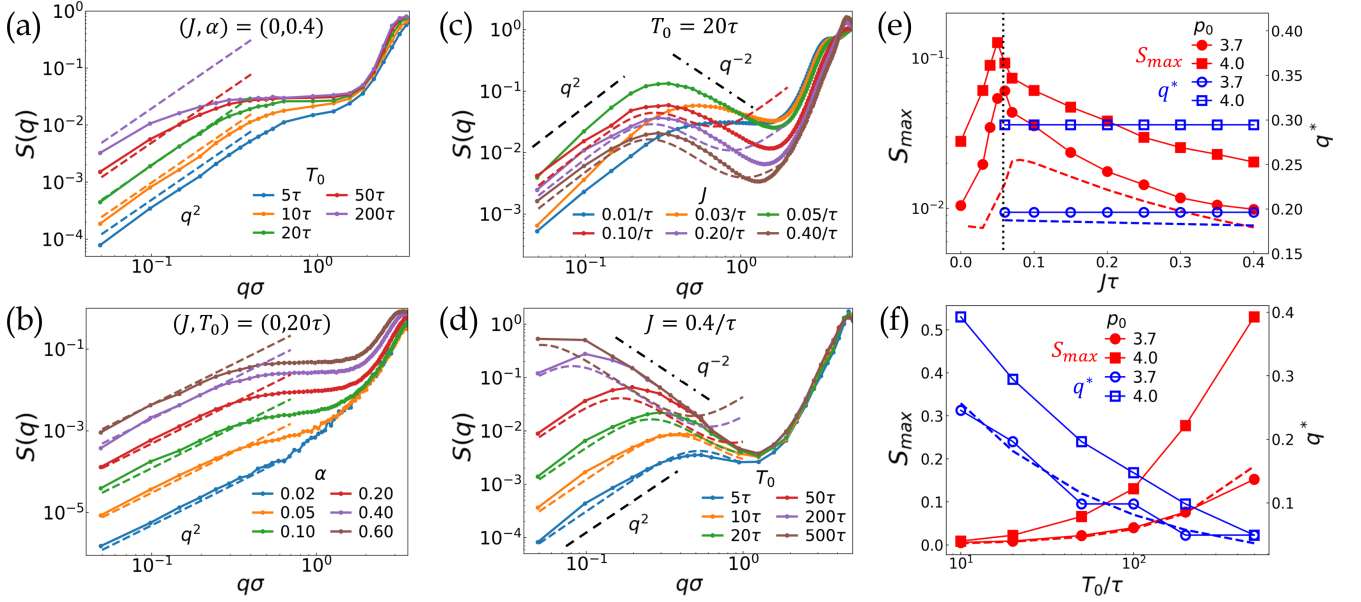


FIG. 3: (a-d) Simulation data (solid symbols) and theoretical predictions (dashed lines) of $S(q)$ for area pulsating systems with: (a) different T_0 at fixed $(p_0, \alpha) = (4.0, 0.4)$ for random pulsation case ($J=0$); (b) different α at fixed $(p_0, T_0) = (4.0, 20\tau)$ for random pulsation case ($J=0$); (c) different J at fixed $(p_0, \alpha, T_0) = (4.0, 0.4, 20\tau)$; (d) different T_0 at fixed $(J, p_0, \alpha) = (0.4\tau^{-1}, 4.0, 0.4)$. In (c) and (d), a correction $\chi=0.25$ is used; (e-f) Simulation data of S_{max} (red solid symbols) and q^* (blue hollow symbols) as well as the corresponding theoretical predictions (dashed lines) for systems with: (e) different J at fixed $(\alpha, T_0) = (0.4, 20\tau)$; (f) different T_0 at fixed $(J, \alpha) = (0.4\tau^{-1}, 0.4)$. Note that no χ correction is used in the theoretical predictions in (e) and (f). Here, $N=16384$ for all simulations. $\gamma=1.1$ and simulation data of M are used for all theoretical predictions.

we plot S_{max} as a function of J for two different p_0 . We find S_{max} exhibits diverging behavior when $J \rightarrow J^*$, which is more pronounced for large p_0 . In Fig. 3d, we further show $S(q)$ for various T_0 in synchronized states with $J=0.4\tau^{-1}$. With increasing T_0 , S_{max} increases and the location of the peak q^* shifts to the small q . This indicates that both the magnitude and length scale of the density heterogeneity diverge when $T_0 \rightarrow \infty$, resulting in giant density fluctuations following the q^{-2} scaling. This mechanism is quite robust, independent of whether the system is in the solid or liquid phase (*SI Appendix*, Fig. S3). It should be mentioned that giant density fluctuations was reported in MDCK monolayer experimentally [43]. Our model is the minimal model that can qualitatively reproduce these phenomena. (Movie. S5).

It should be emphasized that the hyperuniform fluid state induced by cell pulsation is distinct from previously reported effective hyperuniform state corresponding to $\alpha=0$ in our case [49, 50]. As a comparison, in Fig. 4, we plot the structure factor for systems with random pulsation ($\alpha=0.4$) and without pulsation ($\alpha=0$) under $(p_0, T_0) = (3.8, 20\tau)$ under different system sizes. One can see that while the pulsating cellular system show system-size independent q^2 hyperuniform scaling, the non-pulsating cellular system ($\alpha=0$) only shows a certain degree of uniformity. This is further proven by the inset of Fig. 4, where we compare the effective hyperuniformity index $H = S(q \rightarrow 0)/S(q_{peak})$ of two systems. One can see that H of pulsating cell systems vanishes as

the system size increases ($H(N) \sim N^{-1}$), which is a characteristic of a strict hyperuniformity, while H remains the constant in the non-pulsating case. In fact, the non-pulsating system can only show the strict hyperuniformity in the case of zero perimeter modulus ($K_P=0$) due to the equal-area packing of cells [60, 61], which is difficult to achieve in real cell tissue. Moreover, in *SI Appendix*, Fig. S4, we demonstrate that this hyperuniform fluid state is dynamically robust to external perturbation and give the response of hyperuniform fluid state to thermal noise in *SI Appendix*, Fig. S5 which accords with [52]. In the next section, we will reveals the hydrodynamic mechanism that give rise to the hyperuniform fluid state, as well as the giant density fluctuations state.

Fluctuating hydrodynamic theory of pulsating cell tissue To understand the above anomalous density fluctuations, we construct a hydrodynamic theory based on cell density field $\rho(\mathbf{r}, t)$ and pulsating phase field $\varphi(\mathbf{r}, t)$ (*SI Appendix*),

$$\partial_t \rho = \frac{\mu}{\rho_0} \nabla \cdot (\rho \nabla P) + A_\alpha \nabla^2 \eta(\mathbf{r}, t), \quad (3)$$

$$\partial_t \varphi = \Omega + \sqrt{3} \frac{J}{\rho_0} \nabla^2 \varphi + \sqrt{2T_\varphi} \xi(\mathbf{r}, t), \quad (4)$$

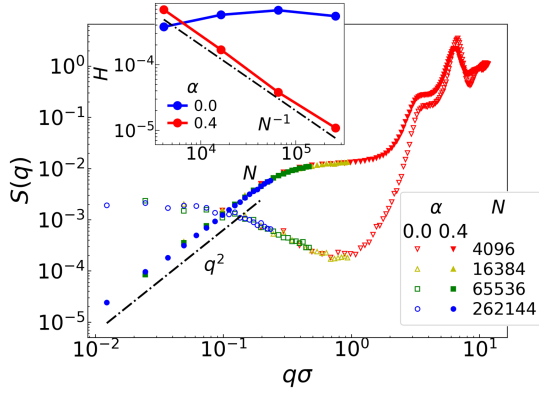


FIG. 4: Finite size effect analysis of static structure factors for the system with random pulsation ($\alpha=0.4$ for solid symbols) and without pulsation ($\alpha=0$ for open symbols). Inset: The effective hyperuniformity index $H=S(q\rightarrow 0)/S(q_{peak})$ as a function of N for the two cases. Other parameters are $(p_0, T_0)=(3.8, 20\tau)$.

where,

$$P(\rho, \varphi, M) = -2K_A \left[\frac{1}{\rho} - \frac{1}{\rho_0} (1 + \alpha M \sin \varphi) \right] + K_P p_0^2 \left(\frac{\sqrt{\rho}}{\sqrt{\rho_0}} - 1 \right) \quad (5)$$

is the local pressure. For a homogeneous state $\rho=\rho_0$, Eq. (5) can be simplified into $P_0 = \frac{2K_A}{\rho_0} \alpha M \sin \varphi$, which reflects that pulsation generates a periodic active stress in the cell tissue that becomes zero in the random pulsating case ($M=0$) under coarse-graining. The second term in Eq. (3) is the center-of-mass conserved noise terms [52, 53, 62] caused by the active reciprocal interaction, i.e., cell pulsation. The noise strength is $A_\alpha = \gamma \alpha (1-M) \sqrt{T_0}$ for small T_0 . Eq. (4) is the coarse-graining of Eq. (2), where $\Omega = 2\pi/T_0$ is the pulsation frequency. η and ξ are uncorrelated Gaussian white noise. By making a weak perturbation around the synchronous homogeneous state, i.e., $\rho(\vec{r}, t) = \rho_0 + \delta\rho(\vec{r}, t)$, $\varphi(\vec{r}, t) = \Omega t + \delta\varphi(\vec{r}, t)$, we obtain equations in the Fourier space with the linear approximation,

$$i\omega \delta\rho_{\omega, \mathbf{q}} = -D' \delta\rho_{\omega, \mathbf{q}} - A_\alpha q^2 \eta_{\omega, \mathbf{q}} - \alpha' q^2 (\delta\varphi_{\omega+\Omega, \mathbf{q}} + \delta\varphi_{\omega-\Omega, \mathbf{q}}) \quad (6)$$

$$i\omega \delta\varphi_{\omega, \mathbf{q}} = -J' q^2 \delta\varphi_{\omega, \mathbf{q}} + \sqrt{2T_0} \xi_{\omega, \mathbf{q}}, \quad (7)$$

where $[\delta\rho_{\omega, \mathbf{q}}, \delta\varphi_{\omega, \mathbf{q}}] = \int dt e^{-i\omega t} \int d\vec{r} e^{-i\vec{q}\cdot\vec{r}} [\delta\rho, \delta\varphi]$. $\alpha' = \frac{\alpha M \mu K_A}{\rho_0}$ is the effective pulsation strength. $J' = \frac{\sqrt{3}}{\rho_0} J$ and $D' = \frac{\mu}{\rho_0} \left(\frac{2K_A}{\rho_0} + \frac{K_P p_0^2}{2} \right)$ are the effective coupling strength and diffusion coefficient respectively. From Eq. (6-7), we can obtain

$$S(q) = 2T_\varphi \frac{\alpha'^2 (J' + D')}{J' D'} \frac{q^2}{(J' + D')^2 q^4 + \Omega^2} + \frac{A_\alpha^2 q^2}{2D_\rho}. \quad (8)$$

In the case of random pulsation ($M=0$ and $\alpha'=0$), $S(q)$ exhibits a q^2 hyperuniform scaling, as a result of the

emergent long-range hydrodynamic correlation [53]. In Fig. 3a-b, we plot the theoretical prediction as the dashed line, which roughly matches the simulation data under different α and T_0 by setting the adjustable parameter $\gamma=1.1$ in A_α . In the case of synchronized state ($M \simeq 1$ and $A_\alpha \simeq 0$), the theory predicts the emergence of the first peak in $S(q)$ at finite T_0 and giant density fluctuations with q^{-2} scaling as $T_0 \rightarrow \infty$. In Fig. 3e-f, we plot S_{max} and q^* of these first peaks as a function of J and T_0 , respectively. One can see that theoretical lines match the simulation data without additional fitting parameter for the synchronized solid phase ($p_0=3.7$). Especially, the theory predicts the right diffusion scaling relationship $q^{*-2} \simeq (J' + D')T_0$. For the large deformation case ($p_0=4.0$), our current theory overestimates the local pressure contributed by the perimeter term. Therefore, a correction $\chi(p_0) < 1$ is needed to match the simulation data (Fig. 3c-d) (*SI Appendix*). From Eq. (8), one can conclude that the center-of-mass conserved noise arising from active reciprocal interaction and periodically driving are two important ingredients to form hyperuniform fluid in the pulsation cellular systems [52, 53, 63–65].

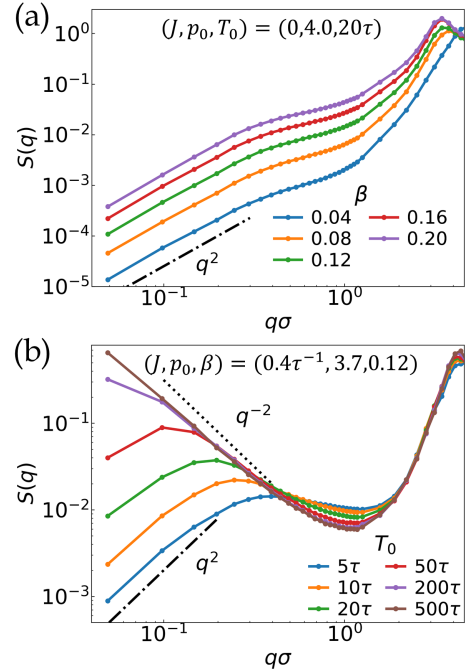


FIG. 5: (a)(b) Simulation data of $S(q)$ for tension pulsating systems with: (a) different β at fixed $(p_0, T_0) = (4.0, 20\tau)$ for random pulsation case ($J=0$); (b) different T_0 at fixed $(J, p_0, \beta) = (0.4\tau^{-1}, 3.7, 0.12)$. Here, $N=16384$ for all simulations.

Generalization to other pulsation form In the above, we focused on cell pulsation driven by volume/area oscillation. Biologically, cell pulsation might also come from fluctuating junction tension [26, 31–35]. Thus, we extend our studies to the case where p_0^i does

stochastic pulsation as

$$p_0^i = p_0 [1 + \beta \cos \varphi_i(t)] \quad (9)$$

while $a_0^i = 1$. Here, β is the pulsating strength. We find a similar cell-pulsation induced hyperuniform fluid state (Fig. 5a and *SI Appendix*, Fig. S6a-b) as well as synchronization-induced dynamical slowdown and giant density fluctuations at large pulsating period (Fig. 5b and *SI Appendix*, Fig. S6c-d). In addition, topological defects in pulsating phase space still mark the structure and dynamic heterogeneity of cell tissue (*SI Appendix*, Fig. S7). Unlike area pulsation, perfectly synchronized tension pulsation is similar to the global cyclic shear, which prevents the synchronous solid state (Movie. S6). Finally, the hydrodynamic theory can also be extended to this pulsating scenario and can qualitatively explain the two anomalous density fluctuations induced by tension pulsation (see *SI Appendix* for discussion). All these results demonstrate the robustness of pulsating activity in determining the fluidization and anomalous density fluctuations in epithelial tissue.

DISCUSSION AND CONCLUSION

In this work, we show that random cell pulsation acting as the reciprocal active force, melts solid epithelial tissues into hyperuniform fluid, while pulsating synchronization induces a reverse solidification. We prove that the pulsation-induced hyperuniform fluid has a strict hyperuniform scaling that can recover from external perturbation. We also prove that the solidification is a BKT-type transition and the birth of topological defects in the pulsating phase space induces strong dynamical and structural heterogeneities at the transition point. We also construct a fluctuation hydrodynamic theory, which can describe two opposite anomalous density fluctuations in a same framework. Our findings deepen our understanding on recently observed giant density fluctuation and topological defects in the MDCK monolayer [25, 27, 28, 43].

In the further, it would be straightforward to incorporate the mechanochemical feedback of cells in our model, which is expected to change the fluidization of tissue and induce other exciting phenomena like density migration waves [18, 28, 66, 67]. It would be interesting to explore fluctuations physics in these more complicated systems. Moreover, it is also tempting to study pulsating cellular systems with nematic order and the relationship between nematic topological defects and tissue flow [68–71]. Such exploration would help us understand how squeezing and contraction forces sculpt cell tissues [72–74] and also guide the design of tissue-like robotic swarms [75].

MATERIALS AND METHODS

Simulation details The model we consider is a 2D confluent cell monolayer composed of N pulsating cells whose area and shape can change with time within a square region L^2 with periodic boundaries. Due to the confluent nature of epithelial tissue, we have $L = \sqrt{NA_0}$ with unit area A_0 . The center of cell i obeys the overdamped dynamics, i.e., $\dot{\mathbf{r}}_i = \mu \mathbf{F}_i$ with μ the mobility coefficient and $\mathbf{F}_i = -\nabla_i E$ the inter-cellular force acting on cell i , where E is the elastic energy of cell tissue. In our simulation, the unit length, unit energy and unit time are defined as $\sigma = \sqrt{A_0}$, $\epsilon = K_A A_0^2$ and $\tau = \sigma^2 / \mu \epsilon$, respectively. Then, the dimensionless energy of the Voronoi model can be written as [6, 76–78]

$$\begin{aligned} \epsilon &= \frac{E}{K_A A_0^2} \\ &= \frac{1}{K_A A_0^2} \sum_i^N [K_A (A_i - A_0^i)^2 + K_P (P_i - P_0^i)^2] \\ &= \sum_i^N \left[\left(\frac{A_i}{A_0} - \frac{A_0^i}{A_0} \right)^2 + \frac{K_P}{K_A A_0} \left(\frac{P_i}{\sqrt{A_0}} - \frac{P_0^i}{\sqrt{A_0}} \right)^2 \right] \\ &= \sum_i^N [(a_i - a_0^i)^2 + \xi (p_i - p_0^i)^2]. \end{aligned}$$

Here, K_A and K_P are the area and perimeter modulus of cells. A_i and P_i are the area and perimeter of cell i , while the corresponding A_0^i and P_0^i are their preferred values. In this energy function, the first term on the right describes the area elasticity of the cell and the second originates from the competition between cell contractility and adhesion tension. $\xi = K_P / (K_A A_0)$ is the dimensionless perimeter modulus. For area pulsation systems, we have $a_0^i = 1 + \alpha \sin \varphi_i$ and $p_0^i = p_0$. For tension pulsation systems, we have $a_0^i = 1$ and $p_0^i = p_0 (1 + \beta \sin \varphi_i)$.

Our simulation starts with a random initial configuration, unless stated otherwise. Then, we use Euler's method to integrate the equation of phase Eq. (2) and the equation of motion with a time step $\Delta t = 0.02\tau$. Fixed $T_\varphi = 0.1\tau^{-1}$ and $T_0 = 200\tau$ are used if no state otherwise. We simulate at least $10,000\tau$ to ensure that the system reaches a dynamically stable state before sampling. The simulation is performed with the number of cells N ranging from 400 to 262,144 depending on the measured quantities and the Voronoi tessellation is based on the C++ library CGAL [79].

Cage relative mean square displacement The dynamic state of cellular monolayers can be accurately characterized by the cage relative mean square displacement of cells, $\text{MSD}_c(t) = \frac{1}{N} \langle \sum_i |\mathbf{u}_i(t) - \mathbf{u}_i^{\text{cage}}(t)|^2 \rangle$, which excludes the disturbance of long-wavelength fluctuations in 2D. Here, $\mathbf{u}_i(t) = \mathbf{r}_i(t) - \mathbf{r}_i(0)$ is the displacement of the cell i over the time period t , and $\mathbf{u}_i^{\text{cage}}(t) =$

$(1/n_i)\sum_{j\in C_i}\mathbf{u}_j(t)$ is the displacement of the ‘cage’ which is composed of n_i adjacent cells. $\langle \rangle$ represents the average over time. The diffusion coefficient can be calculated by $D_c = \lim_{t\rightarrow\infty}[\text{MSD}_c(t)/(4t)]$.

Static structure factor The static structure factor $S(\mathbf{q}) = \frac{1}{N} \left\langle \left| \sum_j e^{i\mathbf{q}\cdot\mathbf{r}_j} \right|^2 \right\rangle$ can be used to characterize the density fluctuations of the system. Here, $\mathbf{q} = [q_x, q_y] = [i\frac{2\pi}{L}, j\frac{2\pi}{L}]$ ($i, j = 1, 2, 3, \dots$) and L is the box size. Then, we project the vector \mathbf{q} to scalar $q = |\mathbf{q}|$ and obtain the results of $S(q)$.

Acknowledgments: The authors thank Ran Ni, Xia-qing Shi and Yan-Wei Li for their careful reading of the manuscript and helpful discussion, and are grateful to the High-Performance Computing Center of Collaborative Innovation Center of Advanced Microstructures, the High-Performance Computing Center (HPCC) of Nanjing University for the numerical calculations. This work is supported by the National Key Research and Development Program of China (No. 2022YFA1405000), the National Natural Science Foundation of China (No. 12275127, 11974175, 12174184, and 12247102). The Innovation Program for Quantum Science and Technology (No. 2024ZD0300101). The Natural Science Foundation of Jiangsu Province (No. BK20233001).

* Electronic address: lql@nju.edu.cn

† Electronic address: myqiang@nju.edu.cn

- [1] Friedl, P. & Gilmour, D. Collective cell migration in morphogenesis, regeneration and cancer. *Nature reviews Molecular cell biology* **10**, 445–457 (2009).
- [2] Hakim, V. & Silberzan, P. Collective cell migration: a physics perspective. *Reports on Progress in Physics* **80**, 076601 (2017).
- [3] Alert, R. & Trepat, X. Physical models of collective cell migration. *Annual Review of Condensed Matter Physics* **11**, 77–101 (2020).
- [4] Park, J.-A. *et al.* Unjamming and cell shape in the asthmatic airway epithelium. *Nature materials* **14**, 1040–1048 (2015).
- [5] Bi, D., Lopez, J., Schwarz, J. M. & Manning, M. L. A density-independent rigidity transition in biological tissues. *Nature Physics* **11**, 1074–1079 (2015).
- [6] Bi, D., Yang, X., Marchetti, M. C. & Manning, M. L. Motility-driven glass and jamming transitions in biological tissues. *Physical Review X* **6**, 021011 (2016).
- [7] Mongera, A. *et al.* A fluid-to-solid jamming transition underlies vertebrate body axis elongation. *Nature* **561**, 401–405 (2018).
- [8] Lin, S.-Z., Ye, S., Xu, G.-K., Li, B. & Feng, X.-Q. Dynamic migration modes of collective cells. *Biophysical journal* **115**, 1826–1835 (2018).
- [9] Giavazzi, F. *et al.* Flocking transitions in confluent tissues. *Soft matter* **14**, 3471–3477 (2018).
- [10] Petrolli, V. *et al.* Confinement-induced transition between wavelike collective cell migration modes. *Physical review letters* **122**, 168101 (2019).
- [11] Peyret, G. *et al.* Sustained oscillations of epithelial cell sheets. *Biophysical journal* **117**, 464–478 (2019).
- [12] Yu, J. *et al.* Spatiotemporal oscillation in confined epithelial motion upon fluid-to-solid transition. *ACS nano* **15**, 7618–7627 (2021).
- [13] Amiri, A., Duclut, C., Jülicher, F. & Popović, M. Random traction yielding transition in epithelial tissues. *Physical Review Letters* **131**, 188401 (2023).
- [14] Barton, D. L., Henkes, S., Weijer, C. J. & Sknepnek, R. Active vertex model for cell-resolution description of epithelial tissue mechanics. *PLoS computational biology* **13**, e1005569 (2017).
- [15] Pasupalak, A., Yan-Wei, L., Ni, R. & Ciamarra, M. P. Hexatic phase in a model of active biological tissues. *Soft matter* **16**, 3914–3920 (2020).
- [16] Cai, L.-b., Ji, W., Luo, J., Lei, Q.-l. & Ma, Y.-q. Numerical study of dynamic zigzag patterns in migrating epithelial tissue. *Science China Physics, Mechanics & Astronomy* **65**, 217011 (2022).
- [17] Tjhung, E. & Berthier, L. Discontinuous fluidization transition in time-correlated assemblies of actively deforming particles. *Physical Review E* **96**, 050601 (2017).
- [18] Zhang, Y. & Fodor, É. Pulsating Active Matter. *Physical Review Letters* **131**, 238302 (2023).
- [19] Manacorda, A. & Fodor, É. Pulsating with discrete symmetry. *arXiv preprint arXiv:2310.14370* (2023).
- [20] Manning, M. L. Essay: Collections of deformable particles present exciting challenges for soft matter and biological physics. *Physical Review Letters* **130**, 130002 (2023).
- [21] Liu, W.-h., Zhu, W.-j. & Ai, B.-q. Collective motion of pulsating active particles in confined structures. *New Journal of Physics* **26**, 023017 (2024).
- [22] Piñeros, W. D. & Fodor, É. Biased ensembles of pulsating active matter. *arXiv preprint arXiv:2403.16961* (2024).
- [23] Banerjee, S., Utuje, K. J. & Marchetti, M. C. Propagating stress waves during epithelial expansion. *Physical review letters* **114**, 228101 (2015).
- [24] Lin, S.-Z., Li, B., Lan, G. & Feng, X.-Q. Activation and synchronization of the oscillatory morphodynamics in multicellular monolayer. *Proceedings of the National Academy of Sciences* **114**, 8157–8162 (2017).
- [25] Hino, N. *et al.* ERK-mediated mechanochemical waves direct collective cell polarization. *Developmental cell* **53**, 646–660 (2020).
- [26] Krajnc, M., Stern, T. & Zankoc, C. Active instability and nonlinear dynamics of cell-cell junctions. *Physical Review Letters* **127**, 198103 (2021).
- [27] Boockock, D., Hino, N., Ruzickova, N., Hirashima, T. & Hannezo, E. Theory of mechanochemical patterning and optimal migration in cell monolayers. *Nature physics* **17**, 267–274 (2021).
- [28] Boockock, D., Hirashima, T. & Hannezo, E. Interplay between mechanochemical patterning and glassy dynamics in cellular monolayers. *PRX Life* **1**, 013001 (2023).
- [29] Pérez-Verdugo, F., Banks, S. & Banerjee, S. Excitable dynamics driven by mechanical feedback in biological tissues. *arXiv preprint arXiv:2310.04950* (2023).
- [30] Pérez-Verdugo, F. & Banerjee, S. Tension Remodeling Regulates Topological Transitions in Epithelial Tissues.

- PRX Life* **1**, 023006 (2023).
- [31] Dierkes, K., Sumi, A., Solon, J. & Salbreux, G. Spontaneous oscillations of elastic contractile materials with turnover. *Physical review letters* **113**, 148102 (2014).
- [32] Curran, S. *et al.* Myosin II controls junction fluctuations to guide epithelial tissue ordering. *Developmental cell* **43**, 480–492 (2017).
- [33] Krajnc, M. Solid–fluid transition and cell sorting in epithelia with junctional tension fluctuations. *Soft Matter* **16**, 3209–3215 (2020).
- [34] Devany, J., Sussman, D. M., Yamamoto, T., Manning, M. L. & Gardel, M. L. Cell cycle–dependent active stress drives epithelia remodeling. *Proceedings of the National Academy of Sciences* **118**, e1917853118 (2021).
- [35] Yamamoto, T., Sussman, D. M., Shibata, T. & Manning, M. L. Non-monotonic fluidization generated by fluctuating edge tensions in confluent tissues. *Soft Matter* **18**, 2168–2175 (2022).
- [36] Duclut, C., Paijmans, J., Inamdar, M. M., Modes, C. D. & Jülicher, F. Active T1 transitions in cellular networks. *The European Physical Journal E* **45**, 29 (2022).
- [37] Solon, J., Kaya-Copur, A., Colombelli, J. & Brunner, D. Pulsed forces timed by a ratchet-like mechanism drive directed tissue movement during dorsal closure. *Cell* **137**, 1331–1342 (2009).
- [38] Martin, A. C., Kaschube, M. & Wieschaus, E. F. Pulsed contractions of an actin–myosin network drive apical constriction. *Nature* **457**, 495–499 (2009).
- [39] Armon, S., Bull, M. S., Aranda-Diaz, A. & Prakash, M. Ultrafast epithelial contractions provide insights into contraction speed limits and tissue integrity. *Proceedings of the National Academy of Sciences* **115**, E10333–E10341 (2018).
- [40] Staddon, M. F., Munro, E. M. & Banerjee, S. Pulsatile contractions and pattern formation in excitable actomyosin cortex. *PLoS Computational Biology* **18**, e1009981 (2022).
- [41] Thiagarajan, R., Bhat, A., Salbreux, G., Inamdar, M. M. & Riveline, D. Pulsations and flows in tissues as two collective dynamics with simple cellular rules. *Isience* **25** (2022).
- [42] Yin, X., Liu, Y.-Q., Zhang, L.-Y., Liang, D. & Xu, G.-K. Emergence, Pattern, and Frequency of Spontaneous Waves in Spreading Epithelial Monolayers. *Nano Letters* **24**, 3631–3637 (2024).
- [43] Zehnder, S. M., Suaris, M., Bellaire, M. M. & Angelini, T. E. Cell volume fluctuations in MDCK monolayers. *Biophysical journal* **108**, 247–250 (2015).
- [44] Zehnder, S. M. *et al.* Multicellular density fluctuations in epithelial monolayers. *Physical Review E* **92**, 032729 (2015).
- [45] Bocanegra-Moreno, L., Singh, A., Hannezo, E., Zagorski, M. & Kicheva, A. Cell cycle dynamics control fluidity of the developing mouse neuroepithelium. *Nature Physics* **1–9** (2023).
- [46] Giavazzi, F. *et al.* Giant fluctuations and structural effects in a flocking epithelium. *Journal of Physics D: Applied Physics* **50**, 384003 (2017).
- [47] Jiao, Y. *et al.* Avian photoreceptor patterns represent a disordered hyperuniform solution to a multiscale packing problem. *Physical Review E* **89**, 022721 (2014).
- [48] Chen, D., Aw, W. Y., Devenport, D. & Torquato, S. Structural characterization and statistical-mechanical model of epidermal patterns. *Biophysical journal* **111**, 2534–2545 (2016).
- [49] Li, X., Das, A. & Bi, D. Biological tissue-inspired tunable photonic fluid. *Proceedings of the National Academy of Sciences* **115**, 6650–6655 (2018).
- [50] Zheng, Y., Li, Y.-W. & Ciamarra, M. P. Hyperuniformity and density fluctuations at a rigidity transition in a model of biological tissues. *Soft Matter* **16**, 5942–5950 (2020).
- [51] Liu, Y., Chen, D., Tian, J., Xu, W. & Jiao, Y. Universal Hyperuniform Organization in Looped Leaf Vein Networks. *Physical Review Letters* **133**, 028401 (2024).
- [52] Lei, Q.-L., Ciamarra, M. P. & Ni, R. Nonequilibrium strongly hyperuniform fluids of circle active particles with large local density fluctuations. *Science advances* **5**, eaau7423 (2019).
- [53] Lei, Q.-L. & Ni, R. Hydrodynamics of random-organizing hyperuniform fluids. *Proceedings of the National Academy of Sciences* **116**, 22983–22989 (2019).
- [54] Shi, X.-q. & Ma, Y.-q. Topological structure dynamics revealing collective evolution in active nematics. *Nature communications* **4**, 3013 (2013).
- [55] Zheng, Z., Hu, G. & Hu, B. Phase slips and phase synchronization of coupled oscillators. *Physical Review Letters* **81**, 5318 (1998).
- [56] Acebrón, J. A., Bonilla, L. L., Vicente, C. J. P., Ritort, F. & Spigler, R. The Kuramoto model: A simple paradigm for synchronization phenomena. *Reviews of modern physics* **77**, 137 (2005).
- [57] Zheng, Z. SYNCHRONIZATION OF COUPLED PHASE OSCILLATORS (2010).
- [58] Li, M.-Y. & Li, Y.-W. Relaxation dynamics in the self-propelled Voronoi model for epithelial monolayers. *Physical Review Research* **6**, 033209 (2024).
- [59] Ansell, H. S., Li, C. & Sussman, D. M. Tunable glassy dynamics in models of dense cellular tissue. *arXiv preprint arXiv:2409.00496* (2024).
- [60] Gabrielli, A., Joyce, M. & Torquato, S. Tilings of space and superhomogeneous point processes. *Physical Review E—Statistical, Nonlinear, and Soft Matter Physics* **77**, 031125 (2008).
- [61] Tang, Y., Li, X. & Bi, D. Tunable Hyperuniformity in Cellular Structures. *arXiv preprint arXiv:2408.08976* (2024).
- [62] Hexner, D. & Levine, D. Noise, diffusion, and hyperuniformity. *Physical review letters* **118**, 020601 (2017).
- [63] Kuroda, Y. & Miyazaki, K. Microscopic theory for hyperuniformity in two-dimensional chiral active fluid. *Journal of Statistical Mechanics: Theory and Experiment* **2023**, 103203 (2023).
- [64] Ikeda, H. Harmonic chain far from equilibrium: single-file diffusion, long-range order, and hyperuniformity. *arXiv preprint arXiv:2309.03155* (2023).
- [65] Ikeda, H. & Kuroda, Y. Continuous symmetry breaking of low-dimensional systems driven by inhomogeneous oscillatory driving forces. *Physical Review E* **110**, 024140 (2024).
- [66] Arzash, S., Tah, I., Liu, A. J. & Manning, M. L. Tuning for fluidity using fluctuations in biological tissue models. *arXiv preprint arXiv:2312.11683* (2023).
- [67] Banerjee, T., Desaleux, T., Ranft, J. & Fodor, É. Hydrodynamics of pulsating active liquids. *arXiv preprint arXiv:2407.19955* (2024).
- [68] Saw, T. B. *et al.* Topological defects in epithelia govern cell death and extrusion. *Nature* **544**, 212–216 (2017).

- [69] Zhang, G. & Yeomans, J. M. Active forces in confluent cell monolayers. *Physical Review Letters* **130**, 038202 (2023).
- [70] Rozman, J., Yeomans, J. M. & Sknepnek, R. Shape-tension coupling produces nematic order in an epithelium vertex model. *Physical Review Letters* **131**, 228301 (2023).
- [71] Chiang, M., Hopkins, A., Loewe, B., Marchetti, M. C. & Marenduzzo, D. Intercellular friction and motility drive orientational order in cell monolayers. *Proceedings of the National Academy of Sciences* **121**, e2319310121 (2024).
- [72] Heisenberg, C.-P. & Bellaïche, Y. Forces in tissue morphogenesis and patterning. *Cell* **153**, 948–962 (2013).
- [73] Dance, A. The secret forces that squeeze and pull life into shape. *Nature* **589**, 186–189 (2021).
- [74] Bailles, A., Gehrels, E. W. & Lecuit, T. Mechanochemical principles of spatial and temporal patterns in cells and tissues. *Annual review of cell and developmental biology* **38**, 321–347 (2022).
- [75] Li, S. *et al.* Particle robotics based on statistical mechanics of loosely coupled components. *Nature* **567**, 361–365 (2019).
- [76] Fletcher, A. G., Osterfield, M., Baker, R. E. & Shvartsman, S. Y. Vertex models of epithelial morphogenesis. *Biophysical journal* **106**, 2291–2304 (2014).
- [77] Alt, S., Ganguly, P. & Salbreux, G. Vertex models: from cell mechanics to tissue morphogenesis. *Philosophical Transactions of the Royal Society B: Biological Sciences* **372**, 20150520 (2017).
- [78] Li, X., Das, A. & Bi, D. Mechanical heterogeneity in tissues promotes rigidity and controls cellular invasion. *Physical review letters* **123**, 058101 (2019).
- [79] Fabri, A. & Pion, S. CGAL: The computational geometry algorithms library. In *Proceedings of the 17th ACM SIGSPATIAL international conference on advances in geographic information systems*, 538–539 (2009).